

THE EFFECT OF DIFFERENT VOLUME-OF-FLUID (VOF) METHODS ON ENERGY DISSIPATION IN SIMULATIONS OF PROPAGATING WAVES

BULENT DUZ*, MART J.A. BORSBOOM[‡], PETER R. WELLENS[‡],
ARTHUR E.P. VELDMAN[†] AND RENE H.M. HUIJSMANS*

*Department of Ship Hydrodynamics
Technical University of Delft
Mekelweg 2, 2628 CD Delft, The Netherlands
e-mail: b.duz@tudelft.nl, r.h.m.huijsmans@tudelft.nl, www.tudelft.nl

[‡]Deltares
P.O. Box 177, 2600 MH Delft, The Netherlands
e-mail: mart.borsboom@deltares.nl, peter.wellens@deltares.nl, www.deltares.nl

[†]Institute for Mathematics and Computer Science
University of Groningen
P.O. Box 407, 9700 AK Groningen, The Netherlands
e-mail: a.e.p.veldman@rug.nl, www.rug.nl

Key words: Volume-of-fluid, Propagating waves, MACHO, COSMIC, Energy dissipation, Free surface advection

Abstract. Spurious energy dissipation in numerical wave simulations due to numerical diffusion is a widely-known problem that can have several causes. The numerical diffusion can be due to the discretisation method used for the governing equations applied inside the flow domain, but can also be due to the numerical implementation of the moving free surface and the boundary conditions applied at the free surface. A technique to model an arbitrary 3D free surface efficiently is the volume-of-fluid (VOF) method. In this paper, the attention is focused on the effect of various VOF methods on spurious wave energy dissipation. For this purpose, we will compare several VOF methods in simulations of propagating waves where strong nonlinear behavior is dominant in the flow. The VOF methods in question are based on two methodologies: Simple Line Interface Calculation (SLIC) and Piecewise Linear Interface Calculation (PLIC). Additionally, a grid convergency study will be performed to better understand the numerical behavior of the methods. In the end, comparisons and discussions will be provided to address how numerical wave energy dissipation can be reduced by implementing more accurate VOF methods.

1 INTRODUCTION

Volume-of-fluid (VOF) methods have been successfully used in computational fluid dynamics (CFD) simulation of interfacial and free surface flows for several decades. Typically, the VOF approach presents a model based on a scalar indicator function to transport the fluid according to the underlying velocity field on a fixed computational mesh. This function is characterized by the volume fraction f occupying one of the fluids within each cell. If a cell is completely filled with one fluid, the volume fraction takes the value of 1, and 0 if only the second fluid is present. The values between these two limits indicate the presence of the interface or free surface.

To advect the volume fraction field in time, the following transport equation is solved,

$$\frac{\partial f}{\partial t} + \mathbf{u} \cdot \nabla f = 0, \quad (1)$$

where \mathbf{u} denotes the fluid velocity. Assuming a solenoidal velocity field (incompressible flow) modeled by $\nabla \cdot \mathbf{u} = 0$, Eq. (1) can alternatively take the form:

$$\frac{\partial f}{\partial t} + \nabla \cdot (\mathbf{u}f) = 0. \quad (2)$$

In the VOF context, the discrete volume fraction field is not smoothly distributed at the interface. On the contrary, it displays sharp discontinuous changes between 0 and 1. To preserve the steep profile of the interface, the explicit location of the interface is locally reconstructed and corresponding volume fluxes are computed to update the the volume fraction field to the next discrete time level using Eq. (2). Thus, the interface reconstruction is the first stage of a VOF method. Using the values of the volume fraction in a compact cell stencil, the orientation and location of the interface in a grid cell can be calculated in a piecewise constant, piecewise linear or piecewise parabolic fashion. Among the three classes, the piecewise linear reconstruction is nowadays the most popular approach, and the methods which fall into this category are usually referred to as Piecewise Linear Interface Calculation (PLIC) methods. For a review of interface reconstruction methods, see, e.g., [1, 2].

Once the interface is reconstructed, the volume fraction field is conservatively advected in time via Eq. (2). This equation can be solved using either an unsplit advection or a direction split advection scheme. Although both strategies have been successfully applied in simulation of interfacial flows, direction split advection schemes are more common in standard VOF methods due to ease of implementation: treating individual velocity components to compute 1D fluxes for a sequence of updates in each spatial direction, as opposed to treating velocity components acting in all directions to compute multidimensional fluxes using inherently difficult geometric tasks. For an analysis on these two advection strategies, see, e.g., [2–4]. Regardless of the strategy for advection, conservation of mass must be satisfied and the resulting volume fraction values must be bounded, $0 \leq f \leq 1$, during the transport process of the volume fraction field.

In this paper, the main objective is to compare the performance of several interface reconstruction/advection combinations in simulations of propagating waves. In these tests, we will use two direction split advection schemes of Leonard et.al. [5] which, to the best knowledge of the authors, have not been used in the context of interfacial or free surface flows. The schemes are Multidimensional Advective-Conservative Hybrid Operator (MACHO) and Conservative Operator Splitting for Multidimensions with Inherent Constancy (COSMIC). Besides these two advection schemes, the Eulerian Implicit-Lagrangian Explicit (EI-LE) scheme explained in [6] has been considered for comparison. We will also compare these methods with the current VOF implementation in the CFD simulation tool ComFLOW, see [7, 8] for an overview of the features of this flow solver. It employs the VOF technique introduced by Hirt and Nichols [9] and a local height function (LHF) to overcome the bottlenecks which originate from this VOF technique such as violation of mass conservation and spurious flotsam and jetsam. For a detailed description of the LHF, see [10].

2 INTERFACE RECONSTRUCTION

In a PLIC-VOF method, the interface in each cell is approximated by a line (or a plane in three dimensions). Within each cell, the approximated interface can be defined by the equation:

$$\mathbf{m} \cdot \mathbf{x} = \alpha, \tag{3}$$

where \mathbf{m} is the local surface normal, \mathbf{x} is the position vector of a point on the interface and α is a constant. Essentially, the interface reconstruction involves two procedures: the determination of \mathbf{m} and α . For a given discrete volume fraction field, \mathbf{m} in each cell is usually calculated using the data from the surrounding cells. However, since the discrete volume fraction field is not smoothly distributed at the interface, computation of \mathbf{m} with high accuracy can be complicated and expensive. Since the CFD tool ComFLOW is specifically designed to simulate extreme wave loading on structures in three dimensions, the required reconstruction method must be considerably cheap and easily applicable in 3D while retaining a reasonable accuracy for estimation of the linear interface, although the present study is mainly focused on 2D problems. Among many techniques that are available in the literature, we will show results for three methods: Youngs' algorithm [11], the least-square gradient (LSG) technique by Rider and Kothe [3] and the Mixed-Youngs-Centered (MYC) implementation of Aulisa et al. [12].

Once the normal vector is known, the planar interface within the cell is located so that local volume conservation is satisfied. In other words, the resulting plane should pass through the cell in such a way that the truncated volume lying below the plane is equal to the exact material volume in that cell. As Eq. (3) suggests, the location of the planar interface results from the computation of α . With the available knowledge of the normal vector \mathbf{m} and the volume fraction f within the cell, we can calculate α either iteratively or analytically. Here, we use the analytical relations derived by Scardovelli and Zaleski [13].

3 INTERFACE ADVECTION

After we determine the orientation and location of the planar interface, the volume fraction field is advected in time via Eq. (2). Among many direction split methods, we will consider the MACHO and COSMIC schemes which can be given in 2D as, the MACHO scheme:

$$\begin{aligned} f^* &= f^n - \Delta t \frac{\partial u f^n}{\partial x} + \Delta t f^n \frac{\partial u}{\partial x}, \\ f^{n+1} &= f^n - \Delta t \left(\frac{\partial u f^n}{\partial x} + \frac{\partial w f^*}{\partial z} \right), \end{aligned} \quad (4)$$

and the COSMIC scheme:

$$\begin{aligned} f^X &= f^n - \Delta t \frac{\partial u f^n}{\partial x} + \Delta t f^n \frac{\partial u}{\partial x}, \\ f^Z &= f^n - \Delta t \frac{\partial w f^n}{\partial z} + \Delta t f^n \frac{\partial w}{\partial z}, \\ f^{n+1} &= f^n - \Delta t \left[\frac{\partial}{\partial x} \left(u \frac{f^n + f^Z}{2} \right) + \frac{\partial}{\partial z} \left(w \frac{f^n + f^X}{2} \right) \right]. \end{aligned} \quad (5)$$

An advantage of the MACHO and COSMIC schemes is that both methods can be readily extended to 3D while the EI-LE scheme does not naturally extend to 3D. A clear advantage of the COSMIC scheme is its inherent symmetric feature [5]. However, the COSMIC scheme requires one additional interface reconstruction in 2D at each time step. In 3D, this scheme becomes even more expensive which makes it necessary to implement a computationally cheap interface reconstruction algorithm.

4 NUMERICAL RESULTS

The order of accuracy of the reconstruction methods used in this work has been extensively studied by various researchers, see, e.g., [2–4, 6, 12, 14]. Therefore, we focus our attention on the following advection tests.

4.1 3D deformation field

In this test problem, a sphere of radius 0.15 and center (0.35, 0.35, 0.35) is immersed in a 3D reversible deformation field inside a unit sized cube. The flow is formed by the velocity field:

$$\begin{aligned} u &= 2\sin^2(\pi x) \sin(2\pi y) \sin(2\pi z) \cos(\pi t/T), \\ v &= -\sin(2\pi x) \sin^2(\pi y) \sin(2\pi z) \cos(\pi t/T), \\ w &= -\sin(2\pi x) \sin(2\pi y) \sin^2(\pi z) \cos(\pi t/T), \end{aligned} \quad (6)$$

where $T = 3$ is used. Due to this velocity field, the sphere undergoes severe deformation until it reaches maximum stretching at $t = 1.5$, then returns to its initial shape and

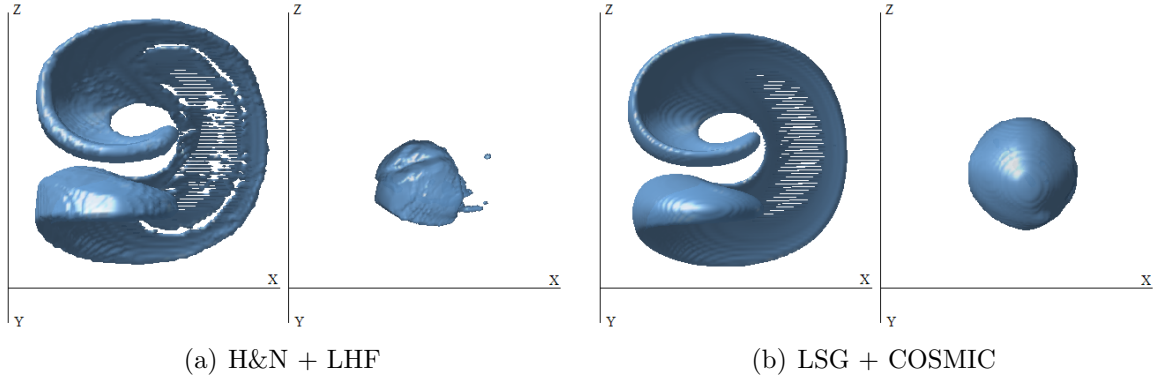


Figure 1: 3D reversible deformation field test on a 128^3 grid at $CFL = 0.5$. Snapshots are taken at maximum deformation ($t = 1.5$), and after the flow returns back ($t = 3$).

position at $t = 3$ by means of the Leveque cosine term [15]. As we employ staggered grid arrangement where the velocity components are defined at cell faces, the velocity field (6) is applied in a discretely divergence-free manner.

Fig. 1 shows the results on a $128 \times 128 \times 128$ grid using the H&N + LHF method versus the LSG + COSMIC combination at time $t = 1.5$ and $t = 3$. The LSG + COSMIC scheme clearly outperforms the H&N + LHF method. However, as the sphere reaches the maximum thinning, holes appear in the deformed fluid body in both results. The recovered shape in the end is roughly a sphere with some minor coalescence when the LSG + COSMIC method is used.

Mesh	Error (Youngs + COSMIC)	Error (LSG + COSMIC)	Error (Youngs + direction-split)	Error (H&N + LHF)
32^3	7.66×10^{-3} 1.56	7.51×10^{-3} 1.68	7.71×10^{-3} 1.47	1.06×10^{-2} 1.05
64^3	2.59×10^{-3} 1.78	2.34×10^{-3} 1.81	2.78×10^{-3} 1.87	5.1×10^{-3} 1.08
128^3	7.50×10^{-4}	6.64×10^{-4}	7.58×10^{-4}	2.4×10^{-3}

Table 1: Errors defined by (7) for the 3D deformation field at $CFL = 0.5$. The order of accuracy of a method is given between the errors. The result on the third column is taken from [4] for comparison.

Tab. 1 shows the the geometrical error E in L_1 which is defined as

$$E = \sum_{i,j,k} \left| f_{i,j,k} - \tilde{f}_{i,j,k} \right| \Delta x_i \Delta y_j \Delta z_k \quad (7)$$

where $\tilde{f}_{i,j,k}$ and $f_{i,j,k}$ are the volume fraction fields at time $t = 0$ and $t = 3$, respectively. In terms of the magnitude of the errors, COSMIC shows a superior performance over the direction-split scheme used in [4] for the same Youngs reconstruction method. Using the LSG method with COSMIC improves the results further.

4.2 Application example: Propagating Rienecker-Fenton waves

The final example is propagating Rienecker-Fenton waves [16] in shallow water. Here, we particularly focus our attention on investigating the effect of various interface-reconstruction /advection combinations on energy dissipation in wave simulations.

4.2.1 Mathematical modeling of the flow solver

If we consider water as a homogeneous, incompressible, viscous fluid, we can describe fluid motion in a three-dimensional domain Ω by the continuity equation and the Navier-Stokes equations in a conservative form as,

$$\oint_{\Gamma} \mathbf{u} \cdot \mathbf{n} \, d\Gamma = 0, \quad (8)$$

$$\begin{aligned} \oint_{\Omega} \frac{\partial \mathbf{u}}{\partial t} d\Omega + \oint_{\Gamma} \mathbf{u} \mathbf{u}^T \cdot \mathbf{n} d\Gamma = \\ -\frac{1}{\rho} \oint_{\Gamma} (p \mathbf{n} - \mu \nabla \mathbf{u} \cdot \mathbf{n}) d\Gamma + \oint_{\Omega} \mathbf{F} d\Omega. \end{aligned} \quad (9)$$

In Eqns. (8) and (9), Ω denotes a volume with boundary Γ and normal vector \mathbf{n} , $\mathbf{u} = (u, v, w)^T$ is the flow velocity, ρ is the fluid density, p is the pressure, μ is the dynamic viscosity, ∇ is the gradient operator and $\mathbf{F} = (F_x, F_y, F_z)^T$ represents external body forces acting on the fluid such as gravity. Detailed explanation of how the individual terms in these equations are treated is beyond the scope of this paper. For this purpose, see, e.g., [17, 18].

4.2.2 Propagating Rienecker-Fenton waves

Four Rienecker-Fenton waves with the same period but different heights are generated, see Tab. 2. Steepness of the waves ranges from 3% to 10.3% which indicates strong nonlinear behavior in the flow. All the three waves are started from rest, and within the first three periods, wave heights are gradually increased until full heights are reached. The length of the domain in the direction of propagation is defined in such a way that the waves do not reach the end of the domain during the simulations. This procedure guarantees that there is no reflection in the computational domain, and hence the solution

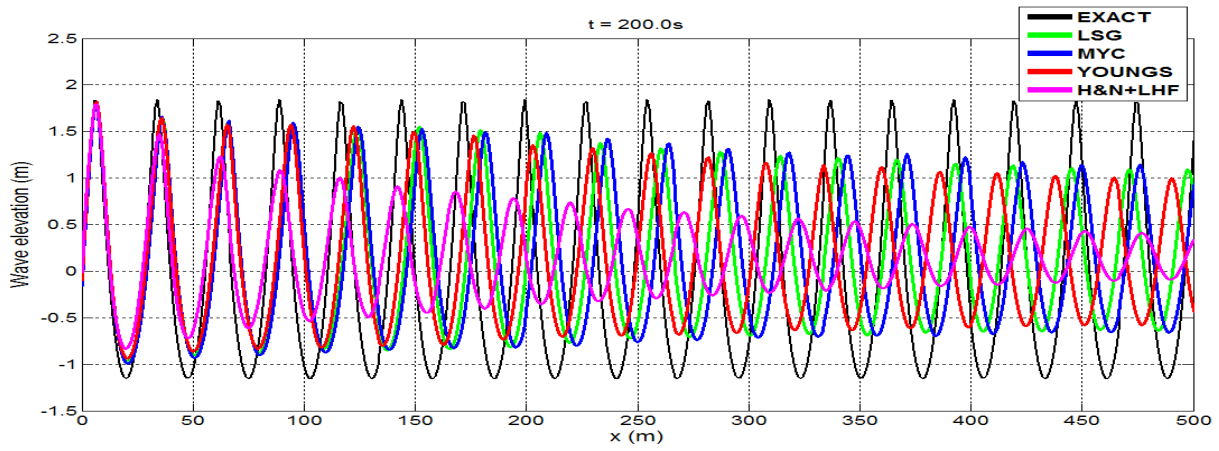
	Rienecker-Fenton waves			
	period	height	length	steepness
	T (s)	H (m)	L (m)	H/L (%)
WAVE3	4	0,75	24,88	3,0
WAVE7	4	2	26,1	7,6
WAVE10	4	3	28,9	10,3

Table 2: Characteristics of the Rienecker-Fenton waves.

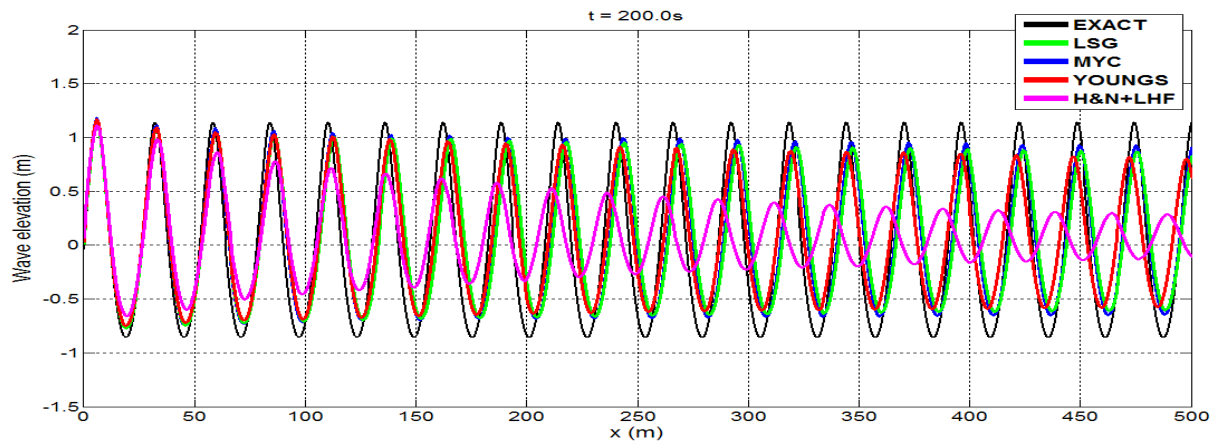
is not perturbed. The duration of the simulations should allow us to have a comprehensive picture regarding wave damping. Therefore, a stable wave system for a large number of wave periods is required. In this analysis, we performed simulations for 200 seconds to have a stable wave system for at least 17 consecutive wave lengths, and correspondingly the domain length is computed as 2000 meters considering the fastest propagating wave component. The water depth in all simulations is 9.5 meters. Two uniform grid resolutions are considered for the grid convergence study: 1.0m and 0.5m in both directions.

Fig. 2 shows the surface elevations as a function of the horizontal position at time $t = 200s$ for the three Rienecker-Fenton waves on the coarse grid, and Fig. 3 on the fine grid. These results are obtained from several PLIC algorithms with the COSMIC advection scheme. Also, the analytical results from the Rienecker-Fenton theory and the Hirt-Nichols' VOF with local height function (H&N + LHF) are plotted in the figures.

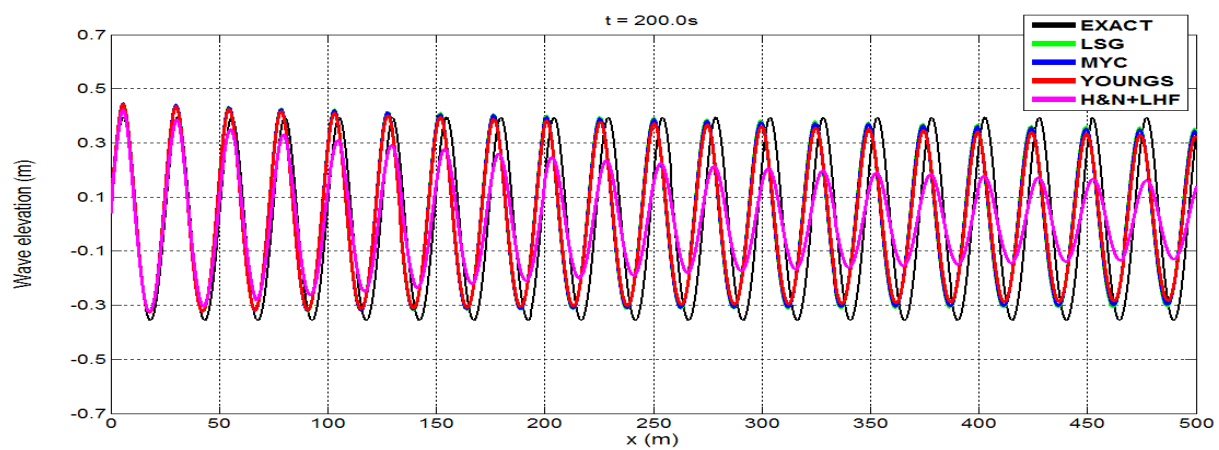
The results on the coarse grid ($\Delta x = \Delta z = 1m$) in Fig. 2 demonstrate that the behavior of the Hirt-Nichols' VOF + LHF is considerably dissipative: WAVE3 lost nearly 59% of the initial wave height after 17 consecutive wave lengths. For WAVE7, this amount is 78%, and for WAVE10 it is 83%. Additionally, this method causes a clear phase shift with respect to the analytical solution. The results indicate that larger phase shifts occur as the steepness of the waves increases. When the PLIC algorithms + COSMIC advection combinations are used, results improve substantially as less dissipation and phase shift are observed. For WAVE3, all the three reconstruction algorithms perform almost the same, somewhat in favor of LSG and MYC. For WAVE7, we observe differences especially as the waves propagate in the computational domain. The Youngs reconstruction algorithm yields the largest wave damping while the LSG and MYC methods perform similarly: 70% of the initial wave height remains with the Youngs method after 17 wave lengths whereas 75% remains with the LSG and MYC methods. In terms of phase shift, there is only a slight difference between the reconstruction methods. In the results for WAVE10, we see that nearly 57% of the initial wave height dissipated when the Youngs method is used. From the LSG and MYC methods, this amount is 51%. After 4 wave lengths from the inflow boundary, we observe three distinct wave signals from the three reconstruction methods.



(a) Results for WAVE10 (steepness: 10.3%)

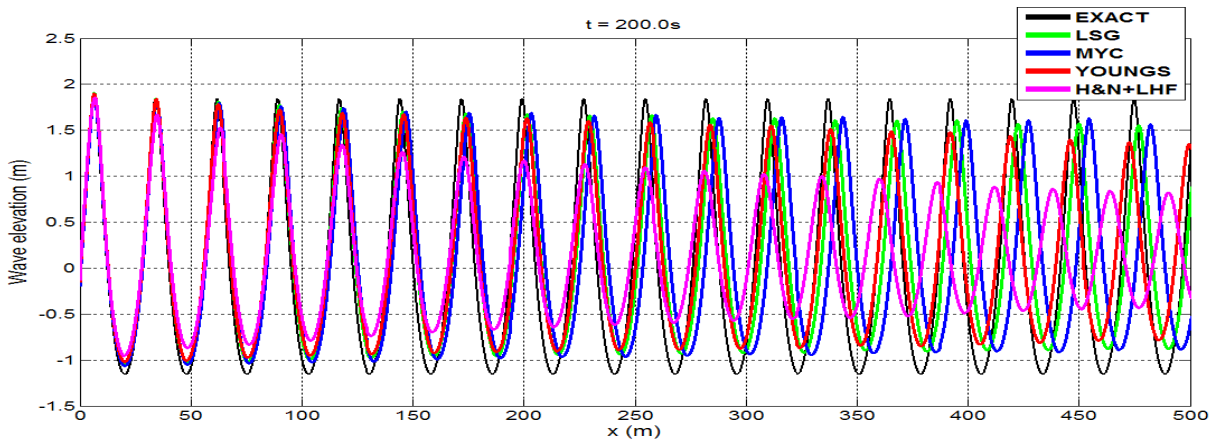


(b) Results for WAVE7 (steepness: 7.6%)

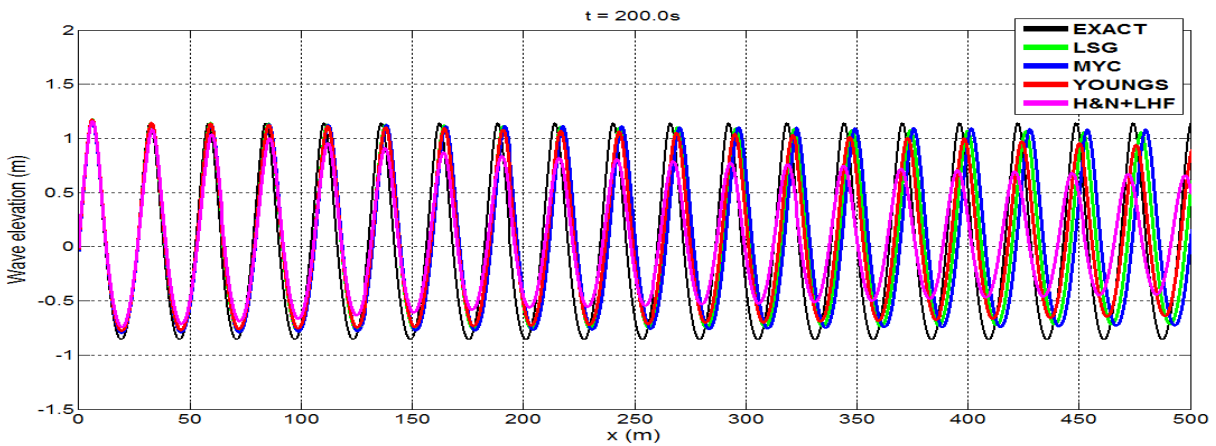


(c) Results for WAVE3 (steepness: 3.0%)

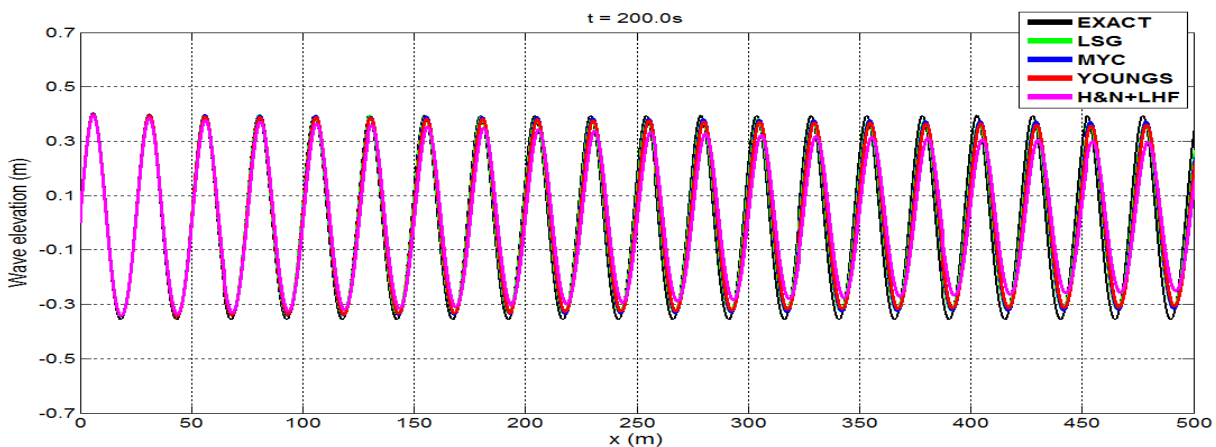
Figure 2: Wave elevations as a function of horizontal location for the waves in Tab. 2. The LSG, MYC and Youngs methods are combined with the COSMIC advection scheme. Grid resolution is $\Delta x = \Delta z = 1m$.



(a) Results for WAVE10 (steepness: 10.3%)

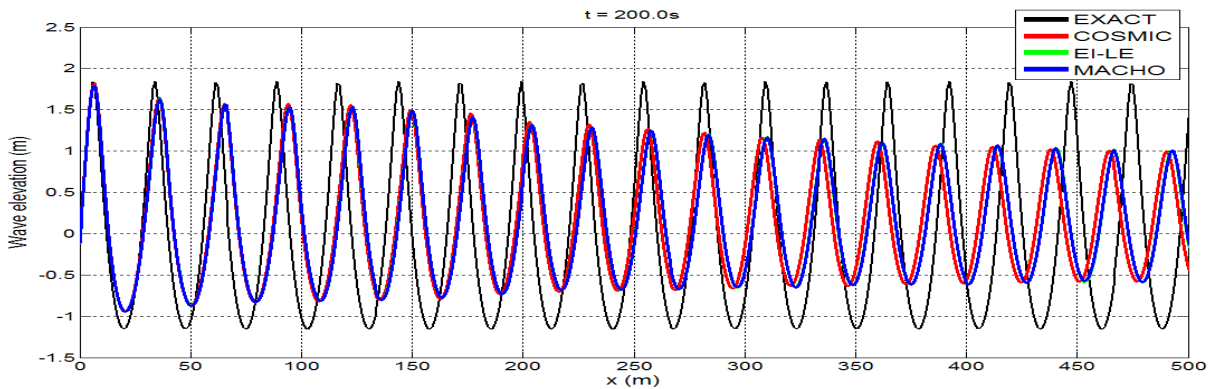


(b) Results for WAVE7 (steepness: 7.6%)

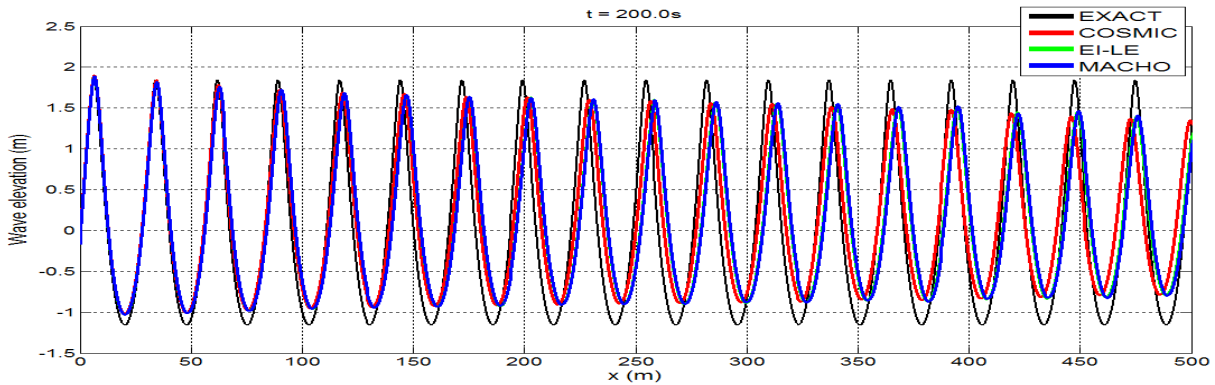


(c) Results for WAVE3 (steepness: 3.0%)

Figure 3: Wave elevations as a function of horizontal location for the waves in Tab. 2. The LSG, MYC and Youngs methods are combined with the COSMIC advection scheme. Grid resolution is $\Delta x = \Delta z = 0.5m$.



(a) Grid resolution is $\Delta x = \Delta z = 1m$



(b) Grid resolution is $\Delta x = \Delta z = 0.5m$

Figure 4: Wave elevations as a function of horizontal location for WAVE10. The COSMIC, EI-LE and MACHO advection schemes are combined with the Youngs reconstruction method.

When the grid resolution is increased ($\Delta x = \Delta z = 0.5m$), significant improvements in the results are noticed, see Fig. 3. When Hirt-Nichols' VOF + LHF is used, WAVE3 lost nearly 26% of its initial wave height after 17 wave lengths, WAVE7 lost 44%, and WAVE10 lost 58%. Similar to the behavior on the coarse grid, H&N + LHF produces substantial errors in terms of phase shift as the steepness increases. With PLIC methods + COSMIC combinations, we observe significant improvements in the results concerning both wave damping and phase shift. For WAVE3, the wave signals obtained with three reconstruction methods are almost the same: 90% of the initial wave height remains with very small phase shift. For WAVE7, 80% of the initial wave height remains with the Youngs method whereas 88% remains with the LSG and MYC methods. Regarding phase shift, the LSG and Youngs method have slight advantage over the MYC method. For WAVE10 we observe clear differences between the three reconstruction methods. When Youngs method is used, only 71% of the initial wave height remains. This amount is 81% with the LSG and MYC methods. The result for WAVE10 also indicate that three wave

signals from the three PLIC methods show different behaviors in terms of phase shift: the MYC method produces the largest phase shift while the Youngs and LSG method produce small phase shifts.

Fig. 4 illustrates the results to compare the performance of the advection schemes. The combinations of the LSG and MYC methods with the MACHO, EI-LE and COSMIC advection schemes resulted in almost the same profiles for the three waves at two grid resolutions. In fact, we observed different wave profiles only when we use the Youngs method with the three advection schemes for the simulation of WAVE10. In case of the WAVE3 and WAVE7, once again we did not notice any differences between the advection methods. Fig. 4 shows that the behavior of the advection methods is almost the same in terms of wave damping, and is only slightly different in terms of phase shift. The difference between the MACHO and EI-LE schemes can be hardly seen at both resolutions while COSMIC produces slightly different wave signals.

5 CONCLUSIONS

We studied the effect of VOF algorithms on spurious energy dissipation in propagating wave simulations. By implementing more accurate interface reconstruction/advection combinations, spurious energy dissipation as well as phase shift are reduced substantially.

Acknowledgment

This research is supported by the Dutch Technology Foundation STW, applied science division of NWO and the technology programma of the Ministry of Economic Affairs in The Netherlands (contracts GWI.6433 and 10475).

REFERENCES

- [1] Benson, D.J. Volume of fluid interface reconstruction methods for multi-material problems. *Appl. Mech. Rev.* (2002) **55**:151–165.
- [2] Pilliod, J.E. and Puckett, E.G. Second-order accurate volume-of-fluid algorithms for tracking material interfaces. *J. Comput. Phys.* (2004) **199**:465–502.
- [3] Rider, W.J. and Kothe, D.B. Reconstructing volume tracking. *J. Comput. Phys.* (1998) **141**:112–152.
- [4] Liovic, P., Rudman, M., Liow, J-L., Lakehal, D. and Kothe, D. A 3D unsplit-advection volume tracking algorithm with planarity-preserving interface reconstruction. *Comput. Fluids* (2006) **35**:1011–1032.
- [5] Leonard, B.P., Lock, A.P. and MacVean, M.K. Conservative explicit unrestricted-time-step multidimensional constancy-preserving advection schemes. *Mon. Weather Rev.* (1996) **124**:2588–2606.

- [6] Scardovelli, R. and Zaleski, S. Interface reconstruction with least-square fit and split Eulerian-Lagrangian advection. *Int. J. Numer. Meth. Fluids* (2003) **41**:251–274.
- [7] Veldman, A.E.P., Luppès, R., Bunnik, T., Huijsmans, R.H.M., Duz, B., Iwanowski, B., Wemmenhove, R., Borsboom, M.J.A., Wellens, P.R., van der Heiden, H.J.L. and van der Plas, P. Extreme wave impact on offshore platforms and coastal constructions. *In Proc. 30th Conf. on Ocean, Offshore and Arctic Engineering OMAE 2011 OMAE2011-49488*.
- [8] Luppès, R., Duz, B., van der Heiden, H.J.L., van der Plas, P. and Veldman, A.E.P. Numerical simulation of extreme wave impact on offshore platforms and coastal constructions. *In Proc. 5th Conf. on Computational Methods in Marine Engineering MARINE 2011*.
- [9] Hirt, C.W. and Nichols, B.D. Volume of fluid (VOF) method for the dynamics of free boundaries. *J. Comput. Phys.* (1981) **39**:201–225.
- [10] Gerrits, J. *Dynamics of liquid-filled spacecraft*. Ph.D. Thesis, University of Groningen, The Netherlands, (2001).
- [11] Youngs, D.L. An interface tracking method for a 3D Eulerian hydrodynamics code. AWRE Design Math. Div. (1987) AWRE/44/92/35.
- [12] Aulisa, E., Manservigi, S., Scardovelli, R. and Zaleski, S. Interface reconstruction with least-squares fit and split advection in three-dimensional Cartesian geometry. *J. Comput. Phys.* (2007) **225**:2301–2319.
- [13] Scardovelli, R. and Zaleski, S. Analytical relations connecting linear interfaces and volume fractions in rectangular grids. *J. Comput. Phys.* (2000) **164**:228–237.
- [14] Wang, Z., Yang, J. and Stern, F. A new volume-of-fluid method with a constructed distance function on general structured grids. *J. Comput. Phys.* (2012) **231**:3703–3722.
- [15] Leveque, R. High-resolution conservative algorithms for advection in incompressible flow. *SIAM J. Numer. Anal.* (1996) **33**:627–665.
- [16] Rienecker, M.M. and Fenton, J.D. A Fourier approximation method for steady water-waves. *J. Fluid Mech.* (1981) **104**:119–137.
- [17] Verstappen, R. W. C. P. and Veldman, A. E. P. Symmetry-preserving discretization of turbulent flow. *J. Comput. Phys.* (2003) **187**:343–368.
- [18] Kleefsman, K. M. T., Fekken, G., Veldman, A. E. P., Iwanowski, B. and Buchner, B. A Volume-of-Fluid based simulation method for wave impact problems *J. Comput. Phys.* (2005) **206**:363–393.